

## Photonic Crystal Composites with Reversible High-Frequency Stop Band Shifts\*\*

By Stephen H. Foulger,\* Ping Jiang, Amanda Lattam, Dennis W. Smith, Jr., John Ballato, David E. Dausch, Sonia Grego, and Brian R. Stoner

Recent widespread application of colloidal crystals in research has attempted to gain fundamental insights into colloidal forces and self-assembly<sup>[1,2]</sup> in addition to providing precursors for the next generation of advanced materials.<sup>[3,4]</sup> One such class of materials that benefits from these systems is dimensionally periodic dielectric structures that exhibit a photonic bandgap, often referred to as photonic crystals.<sup>[5,6]</sup> Colloidal crystals have been exploited in this field since they may undergo self organization at a nanometer length scales, resulting in spatial periodicities that may range from ca.  $10^2$  to  $10^3$  nm.

Two forms of manipulating monodisperse spherical colloidal particles for the generation of photonic crystals have emerged. One approach involves the assembly of the particles into close-packed arrays through sedimentation, and typically relies on non-specific particle–particle “hard sphere” packing to induce order. Particle assembly via this method is attractive in terms of both simplicity and versatility.<sup>[7–12]</sup> The second approach utilizes the long-range electrostatic repulsive interactions of charged colloidal spheres suspended in a liquid medium to produce order.<sup>[2,13,14]</sup> These systems will often adopt a minimum energy crystal structure with either body-centered cubic (bcc) or face-centered cubic (fcc) symmetry,<sup>[1,15,16]</sup> though the ordering in these systems is readily perturbed through minor mechanical disturbances or ionic contamination of the suspending medium.

Approaches to stabilize both inorganic<sup>[17,18]</sup> and organic electrostatically stabilized arrays<sup>[19,20]</sup> through an in-situ polymerization of a monomer around the ordered arrays have been pioneered. These materials have been observed to exhibit a mechanochromic response,<sup>[17,21,22]</sup> where the response has been attributed to an affine deformation of the lattice. Recently, poly(methyl methacrylate) (PMMA) inverse opals

were presented, which exhibited stop-band shifts when the opal was deformed above the glass transition of PMMA.<sup>[23]</sup> Though these approaches have increased the likelihood that these systems may find commercial applications exploiting mechanochromism, the underlying slow recovery time after the cessation of stress or the poor mechanical performance of the photonic crystal is a disadvantage. In this communication, we report on a procedure we have developed that allows for the tailoring of the thermomechanical properties of a photonic crystal to suit end-use criteria, with a specific interest in developing mechanochromic photonic crystal composites that exhibit reversible color variations at deformation frequencies up to 200 Hz.

The first phase in generating a photonic crystal composite requires the stabilization of a crystalline colloidal array composed of monodisperse crosslinked polystyrene spheres dispersed in water (typical characteristics include a diameter of  $109 \pm 26$  nm (mean and standard deviation) and a particle density of  $10^{13}$ – $10^{14}$  cm<sup>-3</sup>) through the encapsulation of the arrays with a photoinitiated free-radical polymerized methacrylate functionalized poly(ethylene glycol) (PEG).<sup>[22,24]</sup> Upon hydrogel encapsulation, the long-range order of the particles is stable to ionic contamination and minor mechanical deformation, though the mechanical performance of the composite is typical of a “soft” hydrogel, which have water contents in excess of 80 vol.-%. The next phase in the composite fabrication requires the removal of water and a re-swelling of the stabilized arrays in a PEG-functionalized acrylate, such as 2-methoxyethyl acrylate (MOEA), a monomer which has a strong affinity for the PEG-based matrix of the hydrogel composite. The incorporation of a small quantity of ethylene glycol dimethacrylate (ca. 1 wt.-%) and a photoinitiator of 2,2-diethoxyacetophenone (DEAP) into the re-swollen system, with subsequent photopolymerization, results in a completely water-free and robust composite.

Figure 1 presents a transmission electron microscopy (TEM) image of a poly(MOEA)-based photonic crystal composite. The order of the particles and the large interparticle distance resulting from their electrostatic stabilization prior to encapsulation is evident. In the case of a lattice which adopts fcc symmetry, the most densely packed planes (i.e., (111) planes) pack parallel to the walls of the container.<sup>[1,16]</sup> The ap-

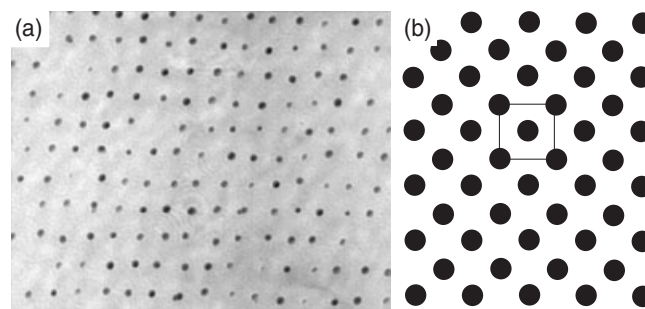


Fig. 1. a) TEM image of poly(MOEA)-based photonic crystal composite (15 K magnification) and b) corresponding schematic of the (100) planes in a fcc crystal. The lattice parameter taken from the TEM image is  $348 \pm 70$  nm.

[\*] Prof. S. H. Foulger, A. Lattam, Prof. J. Ballato  
School of Materials Science and Engineering  
Center for Optical Materials Science and Engineering Technologies  
Clemson University  
Clemson, SC 29634-0971 (USA)  
E-mail: foulger@clemson.edu

P. Jiang, Prof. D. W. Smith, Jr.  
Department of Chemistry  
Center for Optical Materials Science and Engineering Technologies  
Clemson University  
Clemson, SC 29634-0971 (USA)

Dr. D. E. Dausch, Dr. S. Grego, Dr. B. R. Stoner  
MCNC, 3021 Cornwallis Road, PO Box 12889  
Research Triangle Park, NC 27709-2889 (USA)

[\*\*] The authors thank DARPA (Grant Number: N66001-01-1-8938), NASA/EPSCOR (Grant Number: NCC5-575), and the 3M Corporation through a Non-Tenured Faculty Award (SF) for financial support.

proximate diffraction characteristics of these systems can be predicated with the Bragg diffraction equation

$$\lambda_0/2 = n_c d_{hkl} \sin \theta \quad (1)$$

where  $\lambda_0$  is the wavelength of the diffracted light in air,  $d_{hkl}$  is the interplanar spacing,  $n_c$  is the refractive index of the composite, and  $\theta$  is the Bragg angle.<sup>[25]</sup> In the experimental configuration, unpolarized light is propagated along the [111] direction of the fcc lattice, and the observed stop band is then related to the lattice parameter of the conventional cubic unit cell through the Bragg equation and  $a = \sqrt{3}d_{111}$ . The composite employed in Figure 1 exhibits a stop band at 605 nm, which translates into a  $d_{111}$  spacing of 203 nm ( $n_c = 1.489$ ), while  $a$  is 352 nm. The nearest-neighbor distance of the polystyrene particles is 249 nm, over twice their 109 nm diameter. In addition, directly measuring the lattice parameter of the conventional cubic unit cell ( $a$ ) from Figure 1 results in a value of  $348 \pm 70$  nm, in agreement with the reflectance spectra.

The dynamic mechanical analysis (DMA) of photonic crystal composites encapsulated in various polymers is presented in Figure 2. A poly(MOEA)-based system exhibits a low temperature glassy modulus of ca.  $5 \times 10^3$  MPa and undergoes a significant drop at an onset temperature of  $-35$  °C, exhibiting a rubbery modulus of ca. 0.7 MPa. The relaxation exhibited in the dynamic mechanical response of the composite is confirmed by differential scanning calorimetry (DSC), where a maximum change in the heat flow is observed at a temperature of  $-39$  °C. Beyond the rubbery plateau, the modulus is relatively constant up to a temperature of 150 °C, indicative of the crosslinked nature of the matrix.

The photonic crystal composite is composed of a majority of polymerized 2-methoxyethyl acrylate (e.g.,  $\geq 80$  wt.-%). Therefore, the transition temperature of the composite most resembles the “pure” poly(MOEA), where the glass transition ( $T_g$ ) of an uncrosslinked poly(MOEA) has been previously reported in the range of  $-50$  °C to  $-33$  °C.<sup>[26]</sup> The  $T_g$  of the photonic crystal composite can be altered by copolymerization of additional acrylate monomers with MOEA, or through a complete substitution. For instance, substitution of poly(MOEA) with 2-methoxyethyl methacrylate (MOEM) results in a hard and glassy photonic crystal composite at 23 °C, with the glass transition occurring at ca. 40–50 °C, while a 50:50 copolymer of poly(2-methoxyethyl acrylate)-*co*-poly(2-methoxyethyl methacrylate) exhibits a glass-transition that occurs intermediately between the glass transition temperatures of the homopolymers, a feature which is confirmed in the corresponding dynamical mechanical loss characteristics of the photonic crystal composite (cf. Fig. 2).

The ability to tune the  $T_g$  of a photonic crystal composite through a judicious choice of the encapsulation monomer(s) allows for a wide range of coupled optical and mechanical properties. For example, sub-ambient transitions that result in an elastomeric mechanical response of the photonic crystal composite at room temperature allow for the variation of the stop band with stress (i.e., mechanochromic response). It has been previously observed that photonic bandgap materials can exhibit a mechanochromic response,<sup>[17,21,22]</sup> and Figure 3

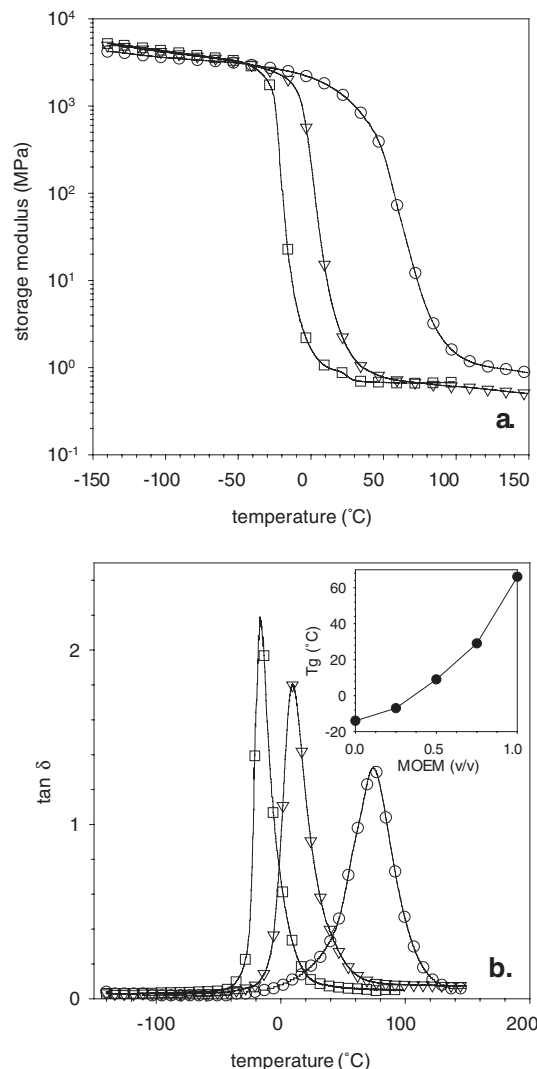


Fig. 2. Dynamical mechanical a) storage modulus ( $E'$ ) and b) loss tangent ( $\tan \delta$ ) of photonic crystal composites encapsulated in poly(MOEA) ( $\square$ ), poly(MOEM) ( $\circ$ ), and 50/50 poly(MOEA-co-MOEM) copolymer ( $\nabla$ ); data acquired at an oscillation frequency of 1 Hz. Inset presents the variation of the observed glass transition computed from the  $\tan \delta$  peaks in MOEA-co-MOEM copolymers with MOEM content.

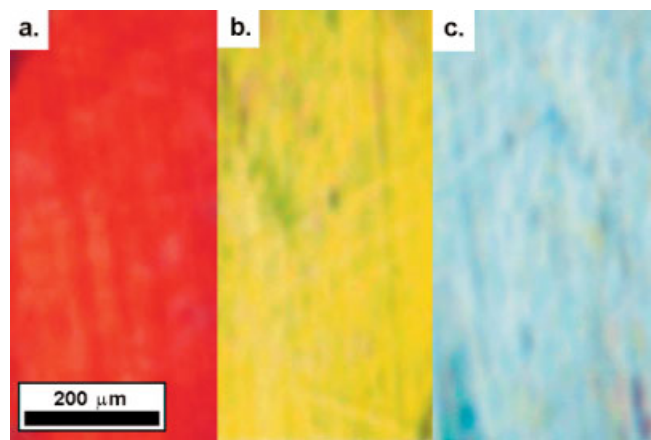


Fig. 3. Reflective characteristics at normal incidence of a poly(MOEA)-based photonic crystal composite at strain levels of a) 0 %, b) 30 %, and c) 48 %. All data were taken at a temperature of 23 °C.

presents the reflection characteristics at normal incidence of a poly(MOEA)-based photonic crystal composite in the stress-free state and at various levels of imposed tensile strain at a temperature of 23 °C. This response has been attributed to the affine deformation of the lattice, where a hypsochromic shift of the stop band is in response to a decrease in the interplanar spacing of the particles. In Figure 4, the orientation of the sample relative to the laboratory frame is schematically pre-

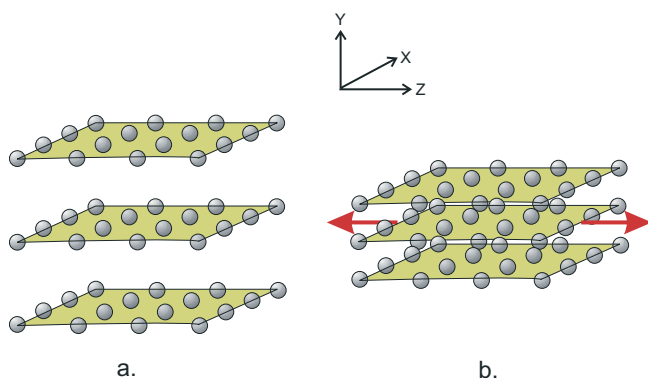


Fig. 4. Orientation of photonic crystal composite relative to laboratory coordinate axis; a) original undeformed state, b) variation in interplanar spacing with uniaxial straining along z-axis. Optical measurements taken along y-axis; changes in particle spacing within the planes are ignored.

sented. In the proposed mechanism, a tensile deformation along the z-axis results in a decrease in the interplanar spacing of the particles along the y-axis. Ignoring any variations in interparticle spacing with straining within a plane of particles, or distortions in the shape of the rigid polystyrene particles, we can rationalize the change in the “color” of the sample presented in Figure 3 with this proposed scheme, where the sample initially appears red in reflection and takes on colors characterized by decreasing wavelengths with increasing tensile strain. Figure 5 presents the reflection characteristics at normal incidence of a poly(MOEA)-based photonic crystal composite in the stress-free state and under a compressive loading along the y-axis. In the initial stress-free state, the position of the stop band is at 610 nm. Upon applying a 145 kPa compressive stress, the stop band shifts down to a wavelength of 517 nm, a 93 nm variation. Assuming no variation in  $n_c$  with deformation, we can calculate the strain associated with the stop band variation through  $\varepsilon_y = \lambda/\lambda_0 - 1$ , where  $\lambda_0$  is the observed stop band wavelength of the unstressed sample. If the stop band can be attributed to the  $d_{111}$  interplanar spacings, the strain associated with the 145 kPa stress is  $-15.2\%$ . At 23 °C, the poly(MOEA)-based photonic crystal composites are at a temperature above their  $T_g$ . Assuming that their mechanical response can be modeled as rubber-like, a composite with a shear modulus of 310 kPa (cf. Fig. 2;  $G \approx E/3$ ) would strain ca.  $-13.5\%$  under a 145 kPa compressive stress, in agreement with the reflectance results. The removal of the compressive stress results in the immediate return of the stop-band position to the original stress-free state (cf. Fig. 5a). In order to investigate this further, a film was uniaxially strained in the DMA at a 9% strain under a 10 Hz sinusoidal oscillation,

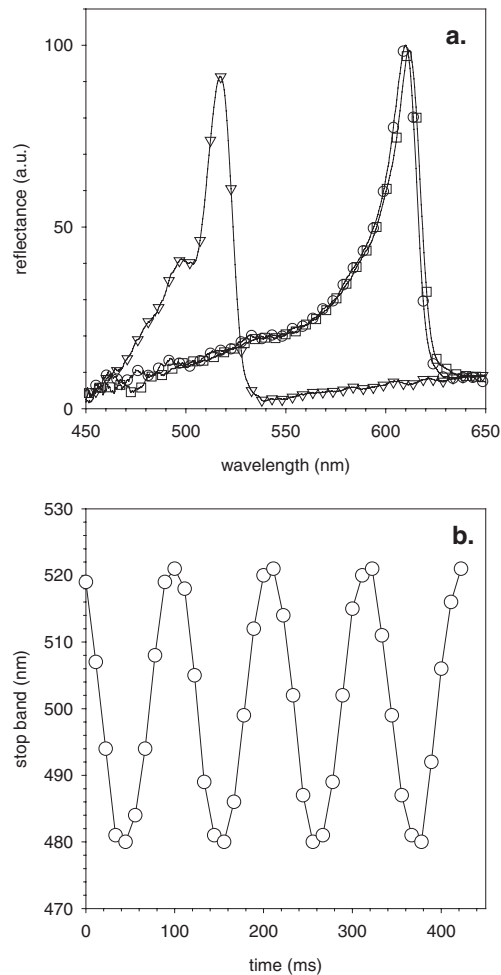


Fig. 5. a) Reflectance spectra of poly(MOEA)-based photonic crystal composite at normal incidence: original stress-free state ( $\square$ ), under a 145 kPa compressive stress ( $\nabla$ ), and unloaded stress-free state ( $\circ$ ). Intensity of curves have been scaled relative to the original stress-free state. b) Variation in observed stop band with cyclic 9% tensile strain of a poly(MOEA)-based photonic crystal composite.

tion, and the resulting stop-band variation is presented in Figure 5b. Preliminary results indicate that no hysteresis in the optical characteristics are introduced with small repeated deformations.

A poly(MOEA)-based photonic crystal composite was coupled directly to a piezoelectric actuator in order to perform a study of the mechanochromic response of the composite in an expanded frequency range. Applying a bias to the piezoelectric actuator placed the composite in a state of stress, where a positive applied voltage resulted in the compression of the photonic crystal composite and a negative voltage placed the composite in tension. Figure 6a presents the change in the position of the observed stop band with actuator bias. Straining the composite in tension resulted in an expansion of the interplanar distance, resulting in a bathochromic shift of the observed stop band, while a compressive strain resulted in a hypsochromic shift. The device exhibited a 172 nm total stop-band tuning range for an applied 240 V span, though the shift in the stop band with bias exhibited a slight

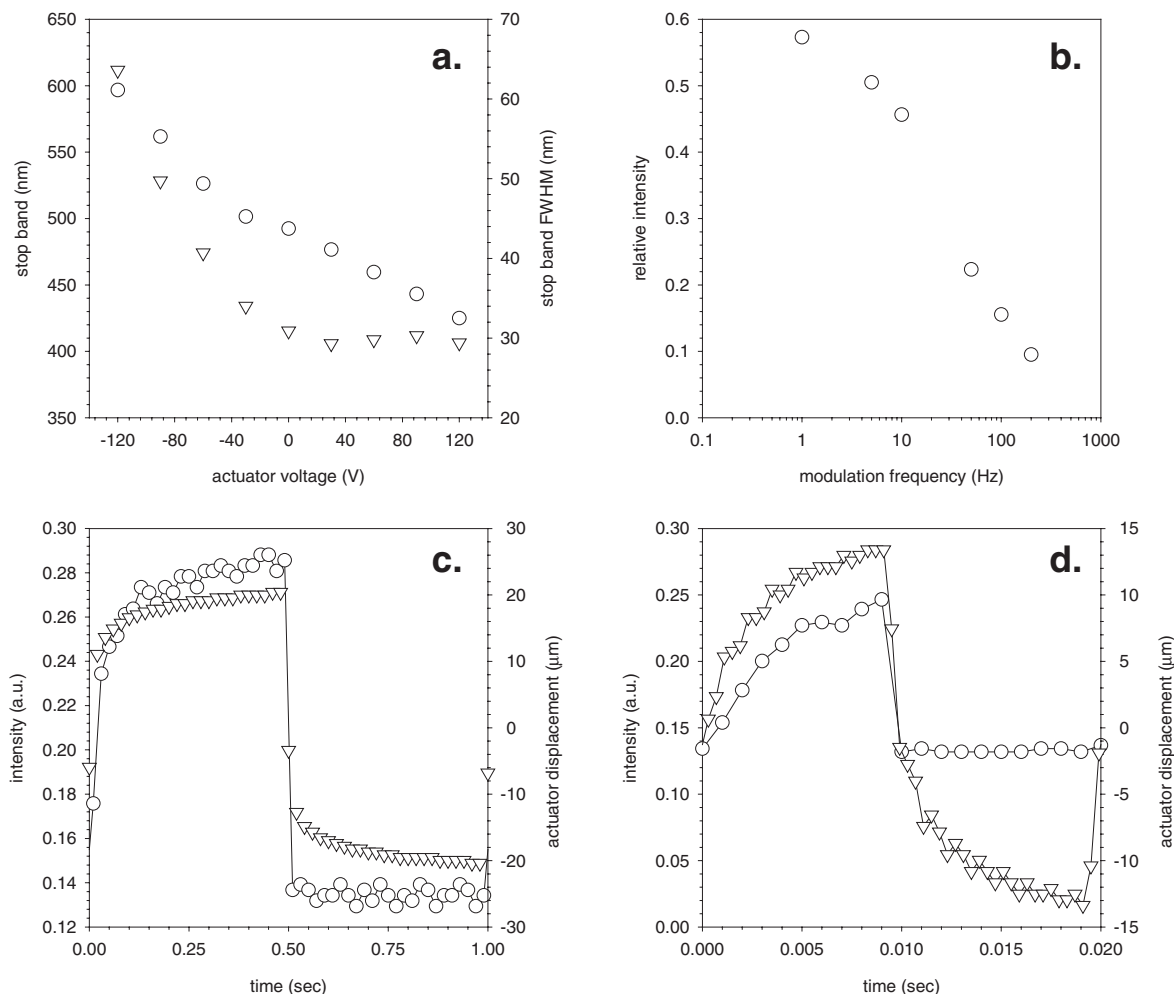


Fig. 6. Optical characteristics of stop-band tuning device composed of coupled photonic crystal composite and piezoelectric actuator: a) Observed stop band (○) and peak FWHM (▽) at various applied bias to the piezoelectric actuator. b) Relative intensity of stop band at 466 nm with increasing frequency of square wave oscillation and  $\pm 60$  V bias to piezoelectric actuator. Peak normalized relative to the intensity of the stop band at a static bias of +60 V; Intensity of reflection peak at 560 nm (○) and actuator displacement (▽) with  $\pm 60$  V bias under a square wave oscillation frequency of c) 1 Hz and d) 50 Hz.

inflection at ca.  $-40$  V (cf. Fig. 6a). In addition, the system exhibited significant peak broadening with increasing tensile deformation, with a ca. 30 nm full width at half maximum (FWHM) at a  $+120$  V bias, increasing to a ca. 70 nm FWHM at a  $-120$  V bias. The increase in the broadness of the peaks is attributed to an introduction of disorder in the spatial periodicity of the arrays with the deformation of the composites. The dynamic tuning characteristic of the composite and actuator coupled device was investigated by utilizing a photonic crystal composite which exhibited a stop band at 508 nm under stress-free conditions. The composite was then strained at a  $+60$  V bias and allowed to come to equilibrium, resulting in a shifted stop band at 466 nm ( $\epsilon_y$  ca.  $-8\%$ ). This procedure was then repeated for a  $-60$  V bias, resulting in a shift of the stop band to 550 nm ( $\epsilon_y$  ca.  $8\%$ ). The actuator was then driven under a square-wave oscillation, employing a  $\pm 60$  V peak-to-peak amplitude and at frequencies between 1 and 200 Hz. Figure 6b presents the resulting peak intensities at a wavelength of 466 nm, normalized by the intensity at equilibrium.

With increasing frequency, the normalized peak intensity is reduced, with observed intensity being less than 10% of the static value at frequencies greater than 200 Hz. At the higher frequencies, the viscoelastic response of the encapsulating poly(MOEA) results in an increase in the storage modulus of the system and a reduced strain in the photonic crystal composite. This response is clearly identifiable in Figures 6c,d where the intensity of the stop band at 560 nm and corresponding actuator displacement is presented for a  $\pm 60$  V bias under a square-wave oscillation at frequencies of 1 Hz and 50 Hz. The actuator displacement is reduced due to the higher modulus of the composite at a frequency of 50 Hz relative to 1 Hz. DMA results indicate an increase of 2.8 times in the storage modulus of the composites as the frequency increases from 1 Hz to 50 Hz; this frequency dependence is a typical behavior of polymers. When no composite was attached to the actuator, the displacement characteristics of the piezoelectric actuator followed the driving square waveform closely. After attaching the composite to the actuator, the viscoelastic na-

ture of the polymeric system appeared to alter the displacement characteristics of the actuator by reducing the rate in which the actuator achieved its maximum displacement. This can be seen in Figure 6c,d as a curvature in the edge of the square wave, a feature which becomes significantly more pronounced at the higher frequency.

In conclusion, an approach to stabilize electrostatically stabilized colloidal arrays through an in-situ polymerization of a monomer around the ordered arrays has allowed the fabrication of photonic crystal composite with a range of thermomechanical properties and coupled optical properties. Composites with sub-ambient glass transitions exhibited reversible mechanochromic characteristics at room temperature. A poly(2-methoxyethyl acrylate)-based photonic crystal composite was coupled directly to a piezoelectric actuator in order to study the static and dynamic stop-band tuning characteristics. The device exhibited a 172 nm total stop-band tuning range and could be modulated up to frequencies of 200 Hz.

## Experimental

Photonic crystal composites were prepared using a procedure described elsewhere [20]. In a typical fabrication run, an opalescing hydrogel based film was removed from its glass slide assembly in which it was fabricated [22] and allowed to air dry for 2 days, then placed in a vacuum oven at 35 °C. The resulting clear film was then swollen in a monomer solution of 2-methoxyethyl acrylate, 2-methoxyethyl methacrylate, or a mixture of the monomers for 2 days. To this solution, ethylene glycol dimethacrylate and DEAP were added and the formulation crosslinked by a 3 min exposure to a UV lamp. All chemicals were purchased from either Aldrich or Acros Organics.

The static reflectance spectra of the composites were collected on an Ocean Optics PC2000 fiber-optic spectrometer with incident light normal to the plate surface. Spectra were collected between the wavelengths of 300 and 900 nm. Reflectance spectra of the composites under dynamic loading conditions were collected with a white light source coupled to a Hamamatsu photomultiplier tube through a bifurcated optical fiber.

Transmission electron microscopy (TEM) was performed with a Hitachi 7000 TEM operating at 100 KV. Samples were prepared by cutting a photonic crystal composite with a diamond knife into sections ca. 100 nm thick and a floating them onto a copper grid. The dynamic mechanical characteristics of the PBG composites were determined with a TA Instruments Dynamic Mechanical Analyzer DMA-2980 operating in the tensile mode. Scans were made at 1 Hz and scanning rate of 5 °C min<sup>-1</sup>. Samples were placed in a vacuum oven at 35 °C for at least 24 h prior to testing.

Received: October 28, 2002  
Final version: December 12, 2002

- [1] Y. Monovoukas, A. P. Gast, *J. Colloid Interface Sci.* **1989**, *128*, 533.
- [2] T. Okubo, *Prog. Polym. Sci.* **1993**, *18*, 481.
- [3] A. A. Zakhidov, R. H. Baughman, Z. Iqbal, C. X. Cui, I. Khayrullin, S. O. Dantas, I. Marti, V. G. Ralchenko, *Science* **1998**, *282*, 897.
- [4] Y. A. Vlasov, N. Yao, D. J. Norris, *Adv. Mater.* **1999**, *2*, 165.
- [5] E. Yablonovitch, *Phys. Rev. Lett.* **1987**, *58*, 2059.
- [6] S. John, *Phys. Rev. Lett.* **1987**, *58*, 2486.
- [7] B. J. Ackerson, S. E. Paulin, B. Johnson, *Phys. Rev. E* **1999**, *59*, 6903.
- [8] Z. Cheng, W. B. Russel, P. M. Chaikin, *Nature* **1999**, *401*, 893.
- [9] J. D. Debord, L. A. Lyon, *J. Phys. Chem. B* **2000**, *104*, 6327.
- [10] J. C. Hulthen, D. A. Treichel, M. T. Smith, M. L. Duval, T. R. Jensen, R. P. van Duyne, *J. Phys. Chem. B* **1999**, *103*, 3854.
- [11] T. Teranishi, M. Hosoe, T. Tanaka, M. Miyake, *J. Phys. Chem. B* **1999**, *103*, 3818.
- [12] J. H. Fendler, *Chem. Mater.* **1996**, *8*, 1616.
- [13] P. A. Hiltner, I. M. Krieger, *J. Phys. Chem.* **1969**, *73*, 2386.
- [14] P. A. Hiltner, Y. S. Papir, I. M. Krieger, *J. Phys. Chem.* **1971**, *75*, 1881.
- [15] N. A. Clark, A. J. Hurd, B. J. Ackerson, *Nature* **1979**, *281*, 57.
- [16] Y. Monovoukas, A. P. Gast, *Phase Transitions* **1990**, *21*, 183.
- [17] J. M. Jethmalani, W. T. Ford, *Chem. Mater.* **1996**, *8*, 2138.

- [18] J. M. Jethmalani, H. B. Sunkara, W. T. Ford, S. L. Willoughby, B. J. Ackerson, *Langmuir* **1997**, *13*, 2633.
- [19] S. A. Asher, J. Holtz, J. Weissman, G. Pan, *MRS Bull.* **1998**, *October*, 44.
- [20] S. H. Foulger, P. Jiang, Y. Ying, A. C. Lattam, D. W. Smith, J. M. Ballato, *Adv. Mater.* **2001**, *13*, 1898.
- [21] S. A. Asher, J. Holtz, L. Li, Z. Wu, *J. Am. Chem. Soc.* **1994**, *116*, 4997.
- [22] S. H. Foulger, P. Jiang, A. C. Lattam, D. W. Smith, J. M. Ballato, *Langmuir* **2001**, *17*, 6023.
- [23] K. Sumioka, H. Kayashima, T. Tsutsui, *Adv. Mater.* **2002**, *14*, 1284.
- [24] S. H. Foulger, S. Kotha, B. Sweryda-Krawiec, T. Baughman, J. M. Ballato, P. Jiang, D. W. Smith, *Optics Lett.* **2000**, *25*, 1300.
- [25] P. A. Rundquist, P. Photinos, S. Jagannathan, S. A. Asher, *J. Chem. Phys.* **1989**, *91*, 4932.
- [26] F. Sun, D. W. Grainger, *J. Polym. Sci., Part A: Polym. Chem.* **1993**, *31*, 1729.

## Virus-Based Alignment of Inorganic, Organic, and Biological Nanosized Materials\*\*

By Seung-Wuk Lee, Soo Kwan Lee, and Angela M. Belcher\*

Functionalized liquid-crystalline materials might provide various pathways to build well-ordered and well-controlled two and three-dimensional structures for the construction of next generation optical, electronic, and magnetic materials and devices.<sup>[1–3]</sup> It has been demonstrated that several types of rod-shape viruses form well-controlled liquid-crystalline phases.<sup>[4,5]</sup> Recently, our group reported a self-assembled ordered nanocrystal film fabrication method using nanocrystal-functionalized M13 virus.<sup>[3]</sup> Through the utilization of genetic engineering techniques, one end of the M13 virus was functionalized to nucleate or bind to a desired semiconductor material. These nanocrystal-functionalized viral liquid-crystalline building blocks were grown into ordered hybrid self-supporting films. The resulting nanocrystal hybrid film was ordered at the nanoscale and at the micrometer scale into 72 μm periodic striped pattern domains. In the previous system, we could easily nucleate and align the nanoparticles for the II–VI semiconductor materials in a one-pot synthetic route. In order to align other materials, including metals and electro-optical materials, biological selection and further evolution are required for each material prior to aligning the nanoparticles. Here, we report a novel nanoparticle alignment method using anti-streptavidin viruses, where the virus was first selected to bind streptavidin protein units. This allows a universal handle for the virus to pick up any material that has been covalently conjugated to streptavidin. Then the self assembling nature of this anti-streptavidin virus can be exploited to make organized hy-

\*] Prof. A. M. Belcher, S. K. Lee  
Department of Materials Science and Engineering and Biological Engineering, Massachusetts Institute of Technology  
Cambridge, MA 02139 (USA)  
E-mail: belcher@mit.edu

S.-W. Lee  
Department of Chemistry and Biochemistry  
Center for Nano- and Molecular Science and Technology  
Texas Materials Institute, The University of Texas at Austin  
Austin, TX 78712 (USA)

\*\*] We acknowledge support from the NSF NIRT program and ARO. We thank Dr. Brent Iverson for helpful discussion.